Available online at www.sciencedirect.com
SCIENCE DIRECT®
Thermochimica Acta 432 (2005) 76–82
thermochimica acta
www.elsevier.com/locate/tca

Enthalpy relaxation in the cooling/heating cycles of polypropylene/organosilica nanocomposites I: Non-isothermal crystallization

V.P. Privalko*, R.V. Dinzhos, E.G. Privalko

Institute of Macromolecular Chemistry, National Academy of Sciences of Ukraine, 02160 Kyiv, Ukraine

Received 9 July 2004; received in revised form 9 September 2004; accepted 24 September 2004
Available online 19 April 2005

Abstract

Non-isothermal crystallization of the neat isotactic polypropylene homopolymer (PP-0) and of a series of nanocomposites (PNC) containing up to 4.68 vol.% of organosilica was studied in the standard DSC mode during constant-rate cooling from the melt state.

Analysis of the nucleation parameters derived from cooling rate dependencies of the temperatures for the onset of crystallization exotherms revealed a slight but systematic increase of the nucleation barrier for lamellar crystallization of PP in the PNC concomitant to stronger restrictions to transport of PP segments across the melt/lamellar crystal interface. The overall crystallization rate data for the PNC were consistent with the assumption of two separate contributions from the initial (unconstrained), and the subsequent (constrained) growth mechanisms, respectively.

The obtained results were considered as evidence for the coexistence in undercooled PP melts of the PNC of initial crystal nucleation and growth sites characteristic for the neat PP-0, and the basically different sites (presumably, PP chains anchored by both ends to the surfaces of two adjacent nanoparticles).

Keywords: Polypropylene nanocomposites; Enthalpy relaxation; Crystallization kinetics

1. Introduction

Polymer *nanocomposites* (PNC) reinforced by relatively small amounts of ultrafine, *nano-disperse* particles (mostly, clay platelets 1 nm thick of an aspect ratio of several hundreds), proved exceptionally promising engineering materials with outstanding mechanical performance, thermal and barrier properties [1–3]. Comprehensive studies of "classical" PNC of polyamide 6/organoclay hybrids have revealed, however, striking similarities of their properties in both melt and solid states [4–6] to those of PNC from isotactic polypropylene melt-compounded with essentially isometric (i.e., of an aspect ratio about unity) nanoparticles of the standard pyrogenic silica (mean particle size $\langle d \rangle \approx 7$ nm), the surface of the latter being pregrafted by γ-irradiation with styrene to minimize the eventual agglomeration effects [7–10]. In the light of these data, it seemed fair to conclude [11] that the significant improvement of, say, mechanical performance of thermoplastic, crystallizable polymers could be expected not only for the PNC containing well-exfoliated organoclay platelets of very high aspect ratio, but also for the PNC filled with more common, isometric nanoparticles (on the condition of preliminary surface treatment of the latter by organic substances to avoid significant agglomeration effects).

Stretching calorimetry studies of such PP/organosilica PNC in the solid state [10,11] revealed the considerable excess of Young's moduli concomitant to the deficit of ther-

* Corresponding author. Tel.: +380 44 559 40 95; fax: +380 44 552 40 64.
E-mail address: privalko@iptelecom.net.ua (V.P. Privalko).

0040-6031/$ – see front matter © 2004 Elsevier B.V. All rights reserved.
doi:10.1016/j.tca.2004.09.023

mal expansivities, limiting strains for elastic behavior and breaking strains compared to reasonable theoretical predictions. These results, combined with the X-ray data, were explained by a model assuming that a non-negligible fraction of PP chains in the melt state would be anchored by each end to the available adsorption-active sites of two different neighboring nanoparticles. The restricted chain mobility in these sites should facilitate the crystal nucleation in the undercooled PP melt; hence, the same PP chain might be involved in two nucleation events at the surfaces of two adjacent nanoparticles. It was believed that subsequent crystallization would result in the oriented, pre-stressed state of tie chains in the interlamellar space of the matrix PP.

Thus, it is the purpose of the present communication to check for a possible influence of such an effect on the crystal nucleation and growth phenomena of these PNC during their continuous cooling from the melt state.

2. Experimental

The neat isotactic polypropylene homopolymer and the nanocomposites containing up to 4.68 vol.% of the standard pyrogenic Aerosil 1380 (Degussa; $\langle d\rangle \approx 7$ nm) pregrafted by γ-irradiation with styrene (samples PP-0, ..., PP-4.68, respectively) were the same as those used in our previous studies [8–11]. As mentioned elsewhere [10], the mean gap between nanoparticles within an infinite cluster of the PP-4.68 nanocomposite ($\langle L\rangle \approx \langle d\rangle[(\varphi_{max}/\varphi)^{1/3} - 1] \approx 8$ nm, where φ is the actual filler volume content and φ_{max} the maximum packing fraction of filler particles) was comparable to the estimated dimensions of PP macromolecular coils in the melt state (that is, about an order of magnitude smaller than the chain contour length corresponding to its full extension).

Enthalpy relaxation in the cooling runs was monitored with the temperature-modulated DSC instrument (Perkin Elmer DSC-2 upgraded and supplied with signal processing software by the IFA GmbH, Ulm). Each sample was initially "overheated" by ~50 K above the apparent melting temperature of PP ($T_m \approx 440$ K), stored for 3 min and cooled in the standard DSC mode to ~360 K at one of the six available constant cooling rates q^- (from 20 K/min down to 0.5 K/min).

3. Results and discussion

3.1. Crystal nucleation

The crystallization exotherms for the PP-0 (Fig. 1a) were the smooth unimodal curves, starting at the temperatures for the onset (i.e., nucleation) of crystallization T_N and passing through the temperatures of maximum crystallization rate at T_{max}; as expected, both T_N and T_{max} decreased, the higher is the cooling rate q^-. The patterns of the cooling rate dependencies of T_N and T_{max} for the PNC (see the representative plots for PP-1.96 in Fig. 1b) were essentially similar; however, the absolute values of both T_N and T_{max} were somewhat different (Table 1).

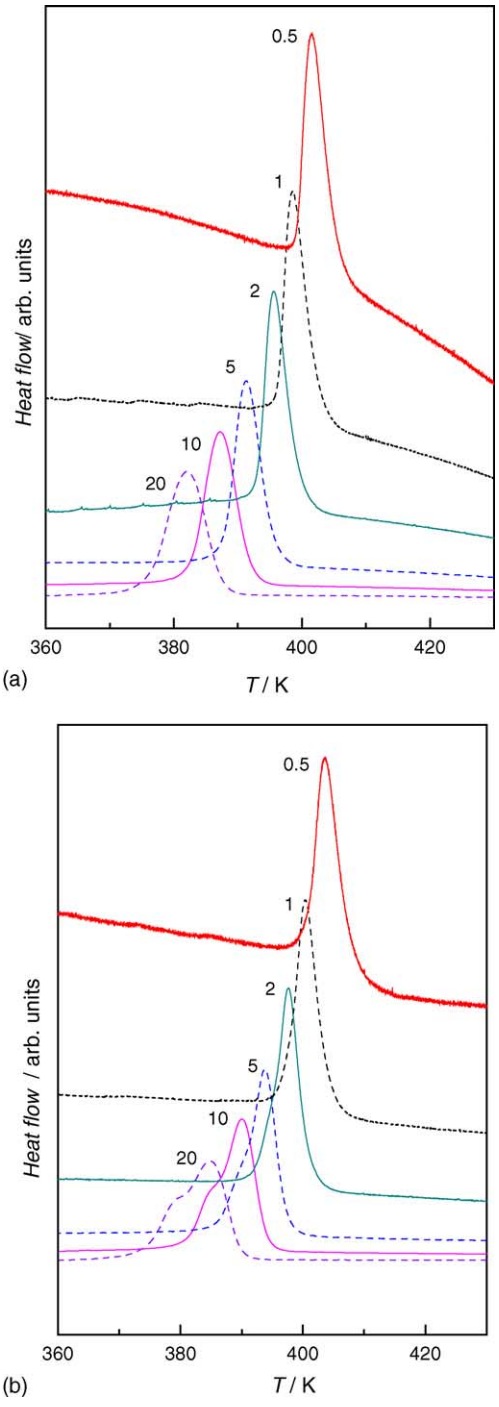

Fig. 1. Crystallization exotherms for PP-0 (a) and PP-1.96 (b); the numbers at the DSC traces refer to the corresponding cooling rates (in K/min).

Table 1
Temperatures (in K) of the onset and of the maximum on crystallization exotherms

Sample	T_N	T_{max}
q^- = 0.5 K/min		
PP-0	409.9	401.7
PP-0.39	409.4	402
PP-0.65	409.1	401.9
PP-1.96	409.0	403.6
PP-4.68	408.4	400.8
q^- = 1 K/min		
PP-0	406.8	398.6
PP-0.39	407.1	399.3
PP-0.65	406.9	399.4
PP-1.96	408.8	400.3
PP-4.68	404.0	397.3
q^- = 2 K/min		
PP-0	403.8	395.7
PP-0.39	404.5	396.6
PP-0.65	405.2	397.0
PP-1.96	405.1	397.6
PP-4.68	402.6	395.7
q^- = 5 K/min		
PP-0	399.3	391.4
PP-0.39	400.2	392.8
PP-0.65	400.4	393.4; 389.9
PP-1.96	401.8	393.7; 390.0
PP-4.68	399,1	394.1; 389.3
q^- = 10 K/min		
PP-0	395.2	387.4
PP-0.39	396.2	389.2; 386.0
PP-0.65	397.2	390.0; 385.4
PP-1.96	397.6	390.2; 385.5
PP-4.68	396.3	390.1; 384.9
q^- = 20 K/min		
PP-0	391.5	382.4
PP-0.39	393.0	384.1; 382.4
PP-0.65	393.0	385.4; 380.4
PP-1.96	394.4	384.7; 380.1
PP-4.68	392.1	384.5; 376.5

As shown elsewhere [12,13], the cooling rate dependencies of T_N should obey the following equation:

$$\ln\left\{\frac{q^-[(m+1)T_N - T_m^0](T_m^0)^m}{T_N^2(\Delta T)^{m+1}}\right\} = \ln\left(\frac{K_m}{a_m}\right) - \frac{a_m(T_m^0)^m}{T_N(\Delta T)^m}, \quad (1)$$

where T_m^0 is the equilibrium melting temperature and ΔH_m° the corresponding melting enthalpy of a hypothetical, "infinitely large" polymer crystal; $\Delta T = T_m^0 - T_N$ the apparent degree of undercooling; $a_m = Z_m/k(\Delta H_m^\circ)^m$ the normalized nucleation parameter; m a dimensionless integer dependent on the mode of nucleation (i.e., $m = 1$, 2 or 4 for the cases of surface, or two-dimensional nucleation; bulk, or three-dimensional nucleation; nucleation in a strained matrix, respectively); Z_m the relevant nucleation barrier; $K_m \sim \exp(-\Delta E/kT_N)$ the normalized molecular transport barrier (usually assumed temperature-invariant in the vicinity of T_m^0); ΔE the corresponding activation enthalpy; k the Boltzmann constant.

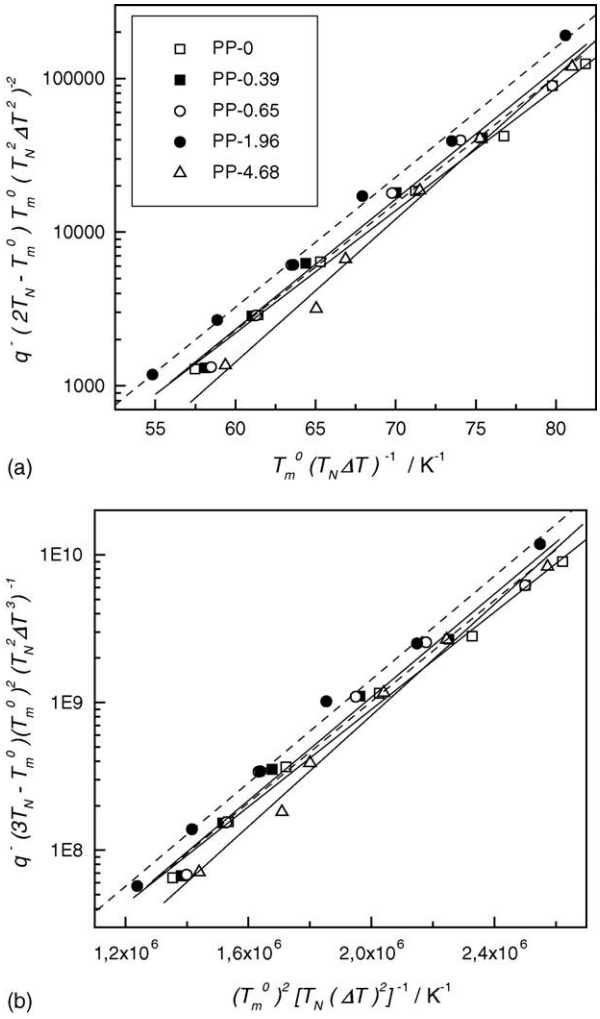

Fig. 2. Fits of the experimental values of T_N at different cooling rates to Eq. (1) assuming $m = 1$ (a) and $m = 2$ (b).

As can be seen from Fig. 2, for all studied samples the quality of the data fits was equally excellent (correlation coefficients $R > 0.99$) for either of the two first nucleation modes (assumed most probable); apparently, the available data are insufficient to distinguish between the two possible nucleation modes. The best-fit values of a_m and K_m are shown in Table 2 (in calculations, $T_m^0 = 461$ K [14] was assumed). Somewhat higher values of a_m for either of nucleation modes in the PNC suggest a slight (but systematic) increase of the

Table 2
Nucleation parameters for non-isothermal crystallization

Sample	a_1 (K)	K_1 (K)	$10^6 a_2$ (K)	K_2 (K)
PP-0	0.175	0.011	3.61	2.13
PP-0.39	0.189	0.0047	3.93	1.47
PP-0.65	0.195	0.0038	4.00	1.37
PP-1.96	0.198	0.0031	4.03	1.28
PP-4.68	0.205	0.0014	4.14	0.80

nucleation barrier for lamellar crystallization of PP within a confined space between neighboring nanoparticles of infinite clusters, while the lower values of K_m (hence, higher apparent values of ΔE), probably, are associated with concomitant stronger restrictions to transport of PP segments across the melt/lamellar crystal interface.

These results can be considered as evidence for the coexistence in undercooled PP melts of the PNC of the initial nucleation sites characteristic for the neat PP-0, and the basically different nucleation sites (presumably, PP chains anchored by both ends to the surfaces of two adjacent nanoparticles [10,11]).

3.2. Overall crystallization kinetics

The smooth, unimodal crystallization exotherms for PP-0 (Fig. 1a) were analyzed in terms of the standard Kolmogorov–Avrami-type equation [12,13,15,16]:

$$\alpha(\theta) = 1 - \exp[-K_n q^n], \quad (2)$$

where $\alpha(\theta)$ is the volume fraction of the melt transformed into crystal at a reduced time θ (in K), K_n the effective rate constant (in K^{-n}), and n the dimensionless shape parameter. As can be seen from the representative plot for the cooling rate $q^- = 20$ K/min (Fig. 3a), the experimental values of $\alpha(\theta) = \Delta H(\theta)/\Delta H_m^\circ$ [where $\Delta H(\theta)$ is the transient value of crystallization heat and $\Delta H_m^\circ = 165.2$ J/g [14] the melting enthalpy of a completely crystalline isotactic PP], could be quantitatively fitted to Eq. (2) with the fitting parameters $K_n = 4.0 \times 10^{-5}$ and $n = 4.61$ only in the range of "primary" crystallization [$\alpha(\theta) < 0.5$], whereas it is the later stages of crystallization which are the issue of our major interest.

In principle, there are several treatments available permitting a quantitative fit of transformation degree over the entire time range of the process [17–19]; however, all these treatments are rather involved. For this reason, a much simpler (albeit more artificial) approach will be used in the present paper. As can be seen from Fig. 3b, the experimental data of Fig. 3a replotted assuming $\alpha(\theta) = \Delta H(\theta)/\Delta H_c$ (where ΔH_c is the total heat of crystallization) are quantitatively fitted to Eq. (2) over the entire range of reduced time θ at not-too-much different values of the fitting parameters ($K_n = 1.0 \times 10^{-5}$ and $n = 5.29$). Similar results were obtained at all other cooling rates; the excellent quality of the data fits can be assessed from the extremely low values of the statistical χ^2 parameter (Table 3).

Most of the best-fitting, non-integer values of the shape parameter n fluctuated within a relatively narrow interval between 4 and 5, as formally consistent with the assumption of identical mechanisms of crystal nucleation and growth over the entire range of q^-. A possible correlation between the derived values of n and the actual shapes of growing crystallization nuclei was considered of little relevance to the aims of this paper and, therefore, not explored in detail (theoretically, $n = 4$ in the case of thermally nucleated spheres; higher values would correspond to bundle-like nuclei [16]). Anyway, judging by the corresponding χ^2 values (see the representative results for $q^- = 20$ K/min in Table 3), the quality of the data fits was not appreciably affected when the best-fit, non-integer values of n were changed for a single, integer value of $n = 5$.

In contrast to PP-0, the crystallization exotherms for the PNC (see the representative plots for the sample PP-1.96 in Fig. 1b) turned out not only considerably broader but also bimodal (especially at high cooling rates), although the areas under the exotherms corrected for PP content (i.e., the neat heats of PP crystallization) remained essentially composition-invariant. Moreover, the values of n decreased, their scatter increased and the overall quality of the data fits to Eq. (2) became worse (i.e., the χ^2 parameters sharply increased), the higher is the q^- (cf. Fig. 4 and Table 3). These results were considered as a further proof of the assumed coexistence of two basically different nucleation sites in undercooled PP melts of the nanocomposites (see above). Therefore, the experimental data for the latter were treated assuming that the overall transformation degree is

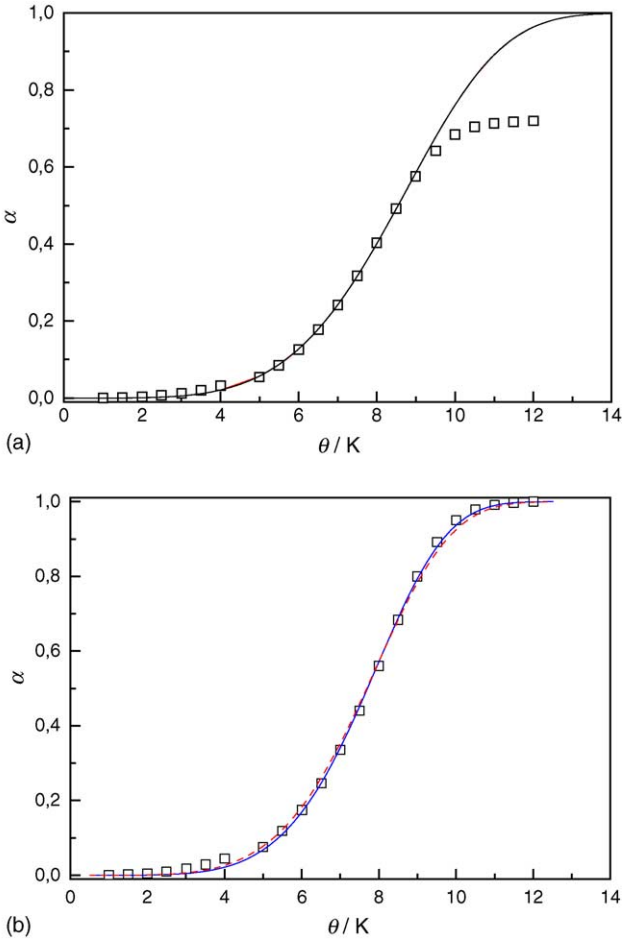

Fig. 3. Fits of the experimental exotherms for PP-0 at $q^- = 20$ K/min to Eq. (2) assuming $\alpha(\theta) = \Delta H(\theta)/\Delta H_m^\circ$ (a) and $\alpha(\theta) = \Delta H(\theta)/\Delta H_c$ (b) for the best-fit, non-integer values of n (solid lines) and $n = 5$ (dashed line).

Table 3
Fitting parameters of Eqs. (2), (2a) and (2b)

q^- (K min^{-1})	Eq. (2)			Eq. (2a)					Eq. (2b)					
	n	$10^5 K_n$ (K^{-n})	$10^5\chi^2$	f	$10^5 K'_n$ (K^{-5})	n''	10^5 K''_n ($K^{-n''}$)	$10^5\chi^2$	f	10^5 K'_n (K^{-5})	n''	$10^5 K''_n$ ($K^{-n''}$)	θ'' (K)	$10^5\chi^2$
PP-0														
0.5	4.56, 5.00	0.84, 0.28	19, 32											
1	4.91	3	17											
2	4.66	6	12											
5	3.97	30	5											
10	3.90	17	5											
20	5.29, 5.00	1, 3	10, 18											
PP-0.39														
0.5	5.50	0.70	6	0.56	2	6.40	0.1	5	0.72	3	3.50	24	4.9	5
1	5.10	2.00	25	0.84	2	3.20	62	25	0.98	2	2.00	12000	1.8	23
2	3.10	290	41	0.47	13	2.42	750	0.79	0.41	10	2.00	10^4	1.6	4
5	2.47	900	23	0.42	18	2.06	1700	31	0.13	23	1.10	3700	1.9	2
10	2.56	480	8	0.39	4	1.97	1600	37	0.15	1	2.20	7000	1.6	3
20	2.83	140	8	0.34	1	2.32	430	2	0.29	0.62	3.31	8000	1.4	4
PP-0.65														
0.5	5.20	2.00	9	0.74	3	5.80	0.46	1	0.55	3	2.17	86	3.9	16
1	5.00	2.00	15	0.30	12	4.10	16	13	0.95	2	1.76	8	3.9	16
2	4.10	14	68	0.79	3	4.10	4	6	0.72	3	4.00	1000	2.2	8
5	3.10	180	70	0.47	10	3.20	100	0.56	0.2	9	3.10	10^4	1.6	10
10	2.50	390	66	0.36	8	2.71	170	1	0.32	8	0.90	500	2.4	0.8
20	2.41	360	36	0.26	6	2.60	170	1	0.1	6	2.50	2500	1.8	2
PP-1.96														
0.5	3.70	70	11	0.60	5	2.30	10^4	2	0.74	5	1.00	3000	1	7
1	5.00	0.50	1	0.68	0.8	6.40	0.5	5	0.46	1	2.80	22	4.2	10
2	4.40	5	23	0.74	2	4.70	1	6	0.51	3	5.70	3000	2.2	2
5	3.70	20	47	0.60	3	4.50	1	2	0.4	4	5.50	2000	2.1	0.7
10	3.10	67	40	0.40	3	3.80	8	0.3	0.18	0.2	4.10	6000	1.7	4
20	2.57	200	16	0.17	6	2.80	100	0.5	0.19	0.2	3.30	6000	1.5	3
PP-4.68														
0.5	3.92	34	3	−0.09	46	3.55	8	0.7	0.36	0.7	2.12	2895	2.0	6
1	4.49	5	3	0.81	3	2.88	208	0.8	0.87	0.3	1.62	5597	2.0	2
2	2.76	419	2	0.06	69	2.90	297	0.6	0.29	3	1.57	8968	2.0	2
5	2.19	997	12	0.36	0.6	2.39	1292	0.4	0.25	0.7	1.62	5822	1.2	1
10	3.01	102	41	0.35	5	3.50	21	0.3	0.60	4	1.94	5162	8.0	0.2
20	2.73	72	81	−0.45	0.5	2.96	47	22	0.55	0.1	1.87	1600	1.0	7

made up of two contributions, each obeying Eq. (2) with its own effective rate constant and shape parameter, as

$$\alpha(\theta) = f[1 - \exp(-K'_n\theta^{n'})] + (1 - f)[1 - \exp(-K''_n\theta^{n''})]. \quad (2a)$$

In Eq. (2a), f and $(1-f)$ are the contributions of the first and second mechanisms (characterized by single-primed and double-primed symbols, respectively); the best-fit values of the relevant parameters are shown in Table 3 (in calculations, $n' = 5$ was assumed for all cooling rates). As could be expected, the overall quality of the data fits to Eq. (2a) was considerably improved (cf. Fig. 4 and Table 3), although in some cases physically unreasonable results ($f < 0$) were obtained. Apparently, the origin of this latter discrepancy is the implicit assumption in Eq. (2a) of the simultaneous onset of both nucleation events, whereas the patterns of crystallization exotherms for the PNC (in particular, the appearance of a second peak at high q^- as seen in Fig. 1b) suggest that the onset and subsequent development of crystallinity by the second growth mechanism somewhat lags behind. To account for this retardation effect, Eq. (2a) was modified further by introducing a correction term θ'' as

$$\alpha(\theta) = f[1 - \exp(-K'_n\theta^{n'})] + (1 - f)\{1 - \exp[-K''_n(\theta - \theta'')^{n''}]\}. \quad (2b)$$

As can be seen from the representative plots for the PNC at $q^- = 20$ K/min (Fig. 4) and from Table 3, the experimental data at all cooling rates excellently fit Eq. (2b) for physically reasonable values of all fitting parameters [in view of the extremely small values of χ^2 parameters for both Eq. (2a) and (2b), the corresponding fitting curves in Fig. 4, in most cases, overlap]. However, as typical for multi-parameter regression analysis, nearly equally excellent fits to Eq. (2b) could be achieved at several widely different values of

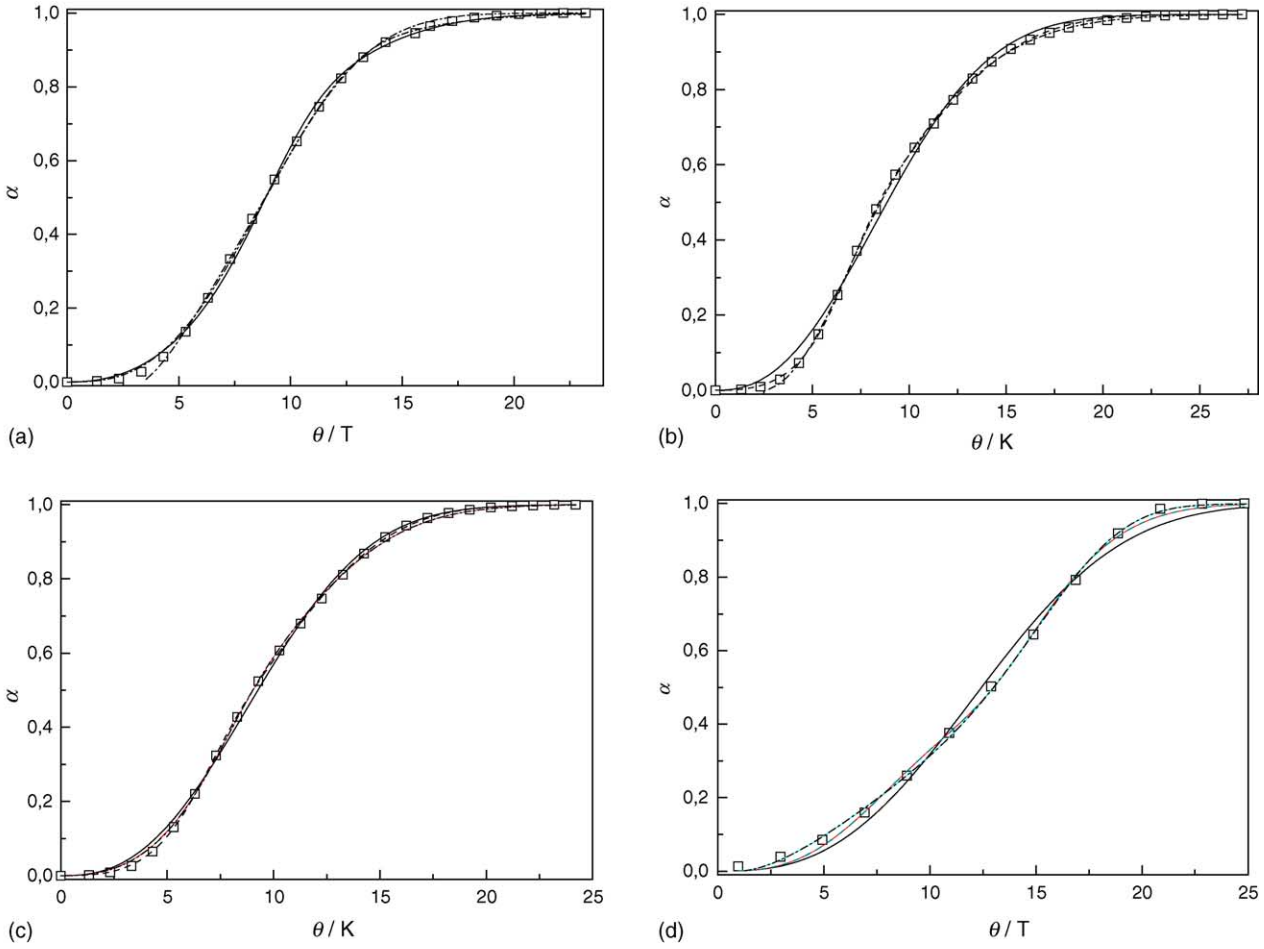

Fig. 4. Fits of the experimental exotherms at $q^- = 20$ K/min to Eq. (2) (solid lines), Eq. (2a) (dashed lines) and Eq. (2b) (dash-dotted lines) for PP-0.39 (a), PP-0.65 (b), PP-1.96 (c) and PP-4.68 (d).

"weak" fitting parameters (in this case, K'_n, K''_n and θ''), whereas the values of a "strong" fitting parameter (n'') remained approximately the same. Anyway, systematically low values of n'' for the PNC decreasing to $n'' \approx 2$ for the sample PP-4.68 imply significant steric constraints for growth of PP lamellae in a confined space within an infinite cluster of organoclay nanoparticles by the second transformation mechanism (compared to $n' = 5$ for an unconstrained growth assumed for the first mechanism). Regrettably, no systematic dependence of the fitting parameters of Eq. (2b) on the organosilica content and/or the cooling rate could be detected; probably, storage during ~3 min at ~490 K before cooling was insufficient to completely erase the structural memory of PP melts in the PNC on previous thermal history.

4. Conclusions

1. Analysis of the nucleation parameters derived from cooling rate dependencies of the temperatures for the onset of crystallization exotherms revealed a slight but systematic increase of the nucleation barrier for lamellar crystallization of PP in the PNC concomitant to stronger restrictions to transport of PP segments across the melt/lamellar crystal interface.
2. The overall crystallization rate data for the PNC were consistent with the assumption of two separate contributions from the initial (unconstrained), and the subsequent (constrained) growth mechanisms, respectively.
3. The obtained results were considered as evidence for the coexistence in undercooled PP melts of the PNC of initial crystal nucleation and growth sites characteristic for the neat PP-0, and the basically different sites (presumably, PP chains anchored by both ends to the surfaces of two adjacent nanoparticles).

Acknowledgements

Thanks are due to the International Bureau of the BMBF (Germany) for a financial support of upgrading the DSC-2 instrument, and to Prof. C. Schick and his group (University of Rostock, Germany) for offering their expertise in operating the temperature-modulated DSC.

References

[1] E.P. Giannelis, Polymer-layered silicates nanocomposites, Adv. Mater. 8 (1996) 29–35.
[2] M. Alexandre, Ph. Dubois, Polymer-layered silicate nanocomposites: preparation, properties and uses of a new class of materials, Mater. Sci. Eng. R28 (2000) 1–63.
[3] T.J. Pinnavaia, G.W. Beall, Polymer–Clay Nanocomposites, Wiley, 2001.
[4] V.M. Karaman, V.F. Shumsky, E.G. Privalko, V.P. Privalko, B. Lehmann, K. Friedrich, Melt viscoelasticity of polyamide 6/organoclay nanocomposites, Polym. Polym. Compos. 11 (2003) 663–668.
[5] V.M. Karaman, V.F. Shumsky, E.G. Privalko, V.P. Privalko, B. Lehmann, K. Friedrich, Viscoelastic behaviour of polyamide 6/organoclay nanocomposites in the melt state, Phys. Condens. Polymer. Syst. (Rivne) (9) (2004) 28–36.
[6] V.P. Privalko, V.M. Karaman, E.G. Privalko, B. Lehmann, K. Friedrich, Structure and thermoelasticity of polyamide 6/organoclay nanocomposites, J. Macromol. Sci. Phys. B42 (2003) 975–987.
[7] V.F. Shumsky, Yu.S. Lipatov, E.G. Privalko, V.M. Karaman, V.P. Privalko, R. Walter, K. Friedrich, M.Z. Rong, Rheological characterization of polypropylene-based nanocomposites in the melt state, Proc. Natl. Acad. Sci. Ukraine (12) (2001) 130–133.
[8] V.F. Shumsky, E.G. Privalko, V.M. Karaman, V.P. Privalko, R. Walter, K. Friedrich, M.Q. Zhang, M.Z. Rong, Viscoelastic behavior of polypropylene-based nanocomposites in the melt state, Adv. Compos. Lett. 10 (2001) 191–195.
[9] V.P. Privalko, V.F. Shumsky, E.G. Privalko, V.M. Karaman, R. Walter, K. Friedrich, M.Q. Zhang, M.Z. Rong, Viscoelasticity and flow behavior of irradiation grafted nano-inorganic particle filled polypropylene composites in the melt state, Sci. Technol. Adv. Mater. 3 (2002) 111–116.
[10] V.P. Privalko, V.M. Karaman, E.G. Privalko, R. Walter, K. Friedrich, M.Q. Zhang, M.Z. Rong, Structure and thermoelasticity of irradiation grafted nano-inorganic particle filled polypropylene composites in the solid state, J. Macromol. Sci. Phys. 41B (2002) 485–503.
[11] V.M. Karaman, Thermo- and viscoelasticity of thermoplastic nanocomposites on the basis of polypropylene and polyamide 6, Ph.D. Thesis, Institute of Macromolecular Chemistry, National Academy of Sciences of Ukraine, Kyiv, 2003.
[12] M. Iguchi, Y. Watanabe, Kinetics of the epitaxy and the overgrowth of polyoxymethylene from molten state on needle-like single-crystals, Brit. Polym. J. 9 (1977) 251–257.
[13] V.P. Privalko, T. Kawai, Yu.S. Lipatov, Crystallization of filled nylon 6 III. Non-isothermal crystallization, Colloid Polym. Sci. 257 (1979) 1042–1048.
[14] B. Wunderlich, Crystal melting, in: Macromolecular Physics, vol. 3, Academic Press, New York, 1980.
[15] T. Ozawa, Kinetics of non-isothermal crystallization, Polymer 12 (1971) 150–158.
[16] B. Wunderlich, Crystal Nucleation growth, annealing, in: Macromolecular Physics, vol. 2, Academic Press, New York, 1976.
[17] S. Hoshino, E. Meinecke, J. Powers, R.S. Stein, S. Newman, Crystallization kinetics of polypropylene fractions, J. Polym. Sci. A 3 (1965) 3041–3066.
[18] I.H. Hillier, Modified Avrami equation for the bulk crystallization kinetics of spherulitic polymers, J. Polym. Sci. A 3 (1965) 3067–3078.
[19] F.P. Price, A phenomenological theory of spherulitic crystallization: primary and secondary crystallization processes, J. Polym. Sci. A 3 (1965) 3079–3086.